Understanding Glucagon Aggregation: In Silico Insights and Experimental Validation

Published Version:
Pisano, R., Arsiccio, A., Collins, V., King, P., Macis, M., Cabri, W., et al. (2024). Understanding Glucagon Aggregation: In Silico Insights and Experimental Validation. MOLECULAR PHARMACEUTICS, 21(8), 3815-3823 [10.1021/acs.molpharmaceut.4c00038].

Availability:
This version is available at: https://hdl.handle.net/11585/980837 since: 2025-02-07

Published:
DOI: http://doi.org/10.1021/acs.molpharmaceut.4c00038

Understanding Glucagon Aggregation: In Silico Insights and Experimental Validation

Roberto Pisano,*,# Andrea Arsiccio,# Valerie Collins,# Patrick King, Marco Macis, Walter Cabri, and Antonio Ricci*

ACCESS | Metrics & More | Article Recommendations | Supporting Information

ABSTRACT: Peptide aggregation poses a significant challenge in biopharmaceutical development and neurodegenerative diseases. This study combines computational simulations and experimental validation to uncover the underlying mechanisms and countermeasures for the aggregation of glucagon, a peptide with a high tendency to aggregate. In silico simulations demonstrate that lactose and 2-hydroxypropyl-β-cyclodextrin (2-HPβCD) influence glucagon aggregation differently: lactose stabilizes glucagon by increasing the α-helical content, while 2-HPβCD disrupts protein–protein interactions. According to the simulations, 2-HPβCD is particularly effective at preserving the monomeric form of glucagon. Experimental validation with microfluidic modulation spectroscopy (MMS) confirms these findings, showing that glucagon in the presence of 2-HPβCD remains structurally stable, supporting the antiaggregation effect of this excipient. This research provides essential insights into glucagon aggregation obtained through a new powerful tool for monitoring the critical properties of peptide aggregation, suggesting new strategies for addressing this challenge in therapeutic peptide development.

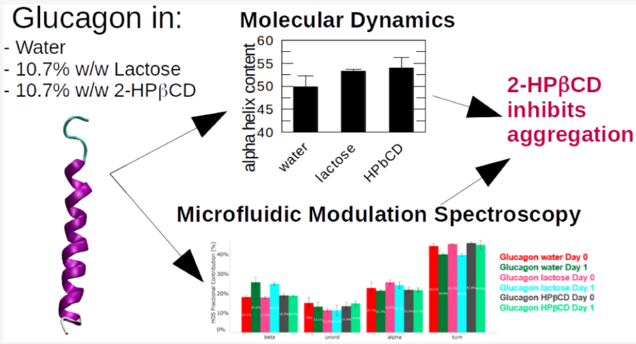

KEYWORDS: *glucagon aggregation, in silico simulations, experimental validation, peptide stability, 2-HPβCD, lactose*

1. INTRODUCTION

Peptide aggregation is a fundamental concern in the field of biochemistry. The propensity of peptides to aggregate, forming amyloid fibrils and misfolded structures, can significantly impact their stability and biological function.[1,2] This phenomenon has attracted significant attention due to its profound implications in various fields, including the development of biopharmaceuticals and the understanding of neurodegenerative diseases. To provide an example, the aggregation of beta-amyloid peptides has been associated with Alzheimer's disease. These beta-amyloid peptides, particularly β-amyloid 42 (Aβ42), tend to aggregate and form insoluble plaques within the brain.[3] These plaque formations are believed to contribute to the deterioration of neurons and the characteristic cognitive decline observed in Alzheimer's disease.[4] The accumulation of these aggregated beta-amyloid peptides remains a distinctive hallmark of Alzheimer's disease pathology.

Additionally, the proclivity of peptides to aggregate has been associated with challenges in the stability and functionality of therapeutic peptides, such as insulin[5] and glucagon.[6] As a result, elucidating the mechanisms of peptide aggregation and developing strategies to inhibit this process have become critical objectives in peptide research.

Peptide aggregation characterization still lacks optimization. Commonly used techniques like size exclusion chromatography (SEC) and ultracentrifugation (UC) have limitations; SEC employs a stationary phase and denaturant solvents like acetonitrile, while UC is not sensitive enough to track small peptide aggregates. A recent study highlighted asymmetric flow field-flow fractionation (Af4) as a potent tool for monitoring the aggregation pattern of peptides under native conditions.[7] However, while Af4 measures the aggregates' size, it does not reveal details about their secondary/tertiary structures. Consequently, having an experimental tool to monitor the structural aspects of aggregates in their native state would complement the understanding of peptide aggregation.

In the case of glucagon, this aggregation tendency has raised substantial challenges in its development as a therapeutic agent for treating severe hypoglycemia.[6−8] Therefore, understanding the mechanisms of peptide aggregation and exploring strategies to mitigate these effects are crucial endeavors. In this article, we investigated the complex issue of glucagon aggregation, utilizing both experimental and computational methods, to shed light on potential solutions to this challenging problem.

Glucagon is a vital peptide hormone consisting of 29 amino acids, and it plays a critical role in regulating glucose levels. Its primary function involves promoting glycogenolysis and gluconeogenesis by binding to the glucagon receptor[9] and, thus, is used for the treatment of severe hypoglycemia associated with diabetes.[10−12]

Glucagon exhibits constraints in terms of both its physical and chemical stabilities, and it has a significant inclination toward aggregation. Mishandling of glucagon has been demonstrated to lead to the formation of amyloidogenic fibrils,[13,14] and this process has been linked to the development of β-sheet structures.[15] The mechanisms underlying the aggregation of glucagon have been extensively investigated. Researchers have explored its behavior in various conditions, including the presence of metals,[16] varying pH levels, and different filtration methods,[17] as well as investigations into new formulations for drug products.[18] Furthermore, numerous scientific studies have examined the morphological changes of glucagon, from its individual monomeric form to oligomeric and fibrillation states.[19,20]

Numerous initiatives have been undertaken to mitigate the risk of aggregation in glucagon. These efforts encompass optimizing its formulation,[18−21] modifying its chemical structure,[22] and creating assays for the detection of aggregates.[23,24]

The primary aim of this research is to investigate the likelihood of glucagon aggregation under different formulation conditions. In addition to proposing alternative methods to prevent aggregation, this study seeks to use computational tools to better understand how a molecule behaves at the molecular level. Furthermore, an innovative microfluidic modulation spectroscopy technique is used to monitor how glucagon clumps together in real time under various conditions, with a focus on its secondary structure. Ultimately, our aim is to link predictions from molecular dynamics simulations with experimental observations.

Regarding the formulation, we investigated the use of lactose and 2-hydroxypropyl-β-cyclodextrin (2-HPβCD) as excipients. 2-HPβCD is composed of seven α-glucopyranose monomers bonded together to create a truncated cone shape. The oxygen atoms in the glucopyranose monomers are connected to hydroxypropyl derivatives, which enhance water solubility and provide amphiphilic properties.[25−27]

Lactose and HPβCD were selected due to their contrasting behaviors. Lactose is repelled from the protein surface, thereby acting as a stabilizer, in line with the preferential exclusion theory.[28,29] In contrast, HPβCD exhibits a preference for interacting with the peptide backbone, effectively acting as a mild denaturant.[30] Furthermore, various authors showed that cyclodextrins serve as protective agents against protein aggregation.[31,32]

To analyze the aggregation of glucagon, a combination of experimental and simulation approaches was employed. The first-generation MMS instrument, created by RedShift BioAnalytics and relying on infrared (IR) spectroscopy, was used for the experimental part. Circular dichroism (CD) is another useful tool for the measurement of protein secondary structures, and is more sensitive to α-helical proteins as it utilizes the differential absorption of left- and right-handed polarized light to make measurements. It is much more difficult to deconvolute spectra when samples contain other types of secondary structures in combination as they often overlay in similar regions of the spectrum and can be positive or negative in magnitude. This is particularly true for two of the most useful types of secondary structures to measure: intramolecular β-sheet and intermolecular β-sheet. The intermolecular β-sheet is especially important to monitor, as it is very commonly associated with structural changes that accompany structural rearrangement leading to aggregation, whereas the intramolecular β-sheet is often part of the natively folded protein. A good example of the utility of quantifying both types of beta-sheets is for stability or formulation experiments in the analysis of monoclonal antibodies (mAbs), whose complex structures contain both inter- and intramolecular beta-sheets.

Additionally, due to the low wavelength of light used for CD measurements, scattering effects are prominent and make measurements difficult in all, but very dilute protein concentrations, without aggregates, and in simple, low-concentration buffers. While employing larger path length cells can help address the first issue, using this method exacerbates the second problem even further. Infrared (IR) spectroscopy of the protein secondary structure does not suffer from any of these problems. Signals for all secondary structures are well-defined and of the same magnitude using transmission measurements, meaning deconvolution is straightforward and secondary structures are quantifiable. Using IR, the wavelengths used for absorbance measurements in the amide I band, the region containing the most information for protein secondary structures, are more than an order of magnitude longer than those for CD (in an approximate range of 5800−6200 nm), meaning scattering effects are very minimal, even with larger complexes or aggregates present. Buffer scattering is also minimal, meaning measurements can be made in situ, at the concentration and in the buffer of interest directly. The major issue with IR spectroscopy of protein secondary structures in the past has been that the signal-to-noise is relatively low compared to some other types of spectroscopy, requiring a relatively high protein concentration for repeatable measurements to be made. By using a powerful and precise quantum cascade laser in combination with a microfluidic rapid referencing method, microfluidic modulation spectroscopy (MMS) solves this problem, and so brings the benefits of IR analysis to a much lower and therefore, more useful range of protein concentrations (0.1 to >200 mg/mL in situ) for the first time.

This experimental analysis was further enhanced by integrating an advanced implicit solvent molecular dynamics technique, specifically designed for examining interactions between proteins and excipients.[33]

2. MATERIALS AND METHODS

2.1. Implicit Solvent Simulations. *2.1.1. Theoretical Background.* The free energy of a solvated protein G^{tot} can be described as the sum of the following contributions:

$$G^{\mathrm{tot}} = E^{\mathrm{vac}} + G^{\mathrm{el}} + G^{\mathrm{np}} + G^{\mathrm{tr}}(c) \quad (1)$$

where E^{vac} is the energy of the protein in vacuum, which results from both internal contributions (bond and angle stretching and dihedral angle interactions) and van der Waals energy terms. G^{np} is the contribution from nonpolar solvation in pure water, i.e., the free energy of hydration for a molecule from which all charges have been removed. G^{el} is the electrostatic part, calculated as the free energy for turning on the partial charges in the solution. These first three terms describe a protein in pure water. The term $G^{tr}(c)$ is used to take into account the presence of cosolutes at a concentration c, and is based on the free energy of transfer approach MIST (model with implicit solvation thermodynamics), that was recently developed.[33]

The generalized Born equation[34] was employed to compute G^{el}, using the OBC(II) model[35] to estimate the Born radii. The dielectric constant was set to 78.4, which is the value for water at 298 K according to the equations by Bradley and Pitzer.[36]

The nonpolar contribution G^{np} was expressed as,

$$G^{np} = \gamma \mathrm{SASA} \tag{2}$$

where γ is the surface tension, while SASA is the total solvent accessibility of the protein. In this study, a specific value of γ, which is 5 cal mol^{-1} Å^{-2}, was employed.[37]

The transfer free energy term $G^{tr}(c)$, that considers the effect of cosolutes, is described as,[33]

$$G^{tr}(c) = \sum_{k=1}^{n_r} g_{k,sc}^{tr}(c)\alpha_{k,sc} + g_{bb}^{tr}(c) \sum_{k=1}^{n_r} \alpha_{k,bb} \tag{3}$$

where the summations run over the n_r residues of the protein, and $g_{k,sc}^{tr}(c)$ and $g_{bb}^{tr}(c)$ are the amino acid side chain (subscript sc) and backbone (subscript bb) contributions, respectively.

For $G^{tr}(c)$, each contribution is weighed by the fractional solvent accessible surface area SASA_k of residue k,

$$\alpha_k = \frac{\mathrm{SASA}_k}{\mathrm{SASA}_{k,\mathrm{Gly}-k-\mathrm{Gly}}} \tag{4}$$

where $\mathrm{SASA}_{k,\mathrm{Gly}\text{-}k\text{-}\mathrm{Gly}}$ is the solvent accessibility of residue k in the tripeptide Gly−k−Gly. The fractional solvent accessible surface area α_k was calculated using the fast algorithm proposed by Hasel et al.[38] The script for the computation of the fractional solvent accessible surface area and of the energetic term $G^{tr}(c)$ is currently part of the 2.8 version of PLUMED as a separate module called SASA.

2.1.2. Simulation Protocol. The Amber 99SB-ILDN force field[39] was used to describe the behavior of glucagon (PDB ID: 1GCN,[40] Figure 1a) under specific conditions. Simulations were carried out at pH 2.7 with a net charge of +4. The AMBER 20 simulation suite,[41] in combination with PLUMED 2.4.7,[42] was employed for this purpose.

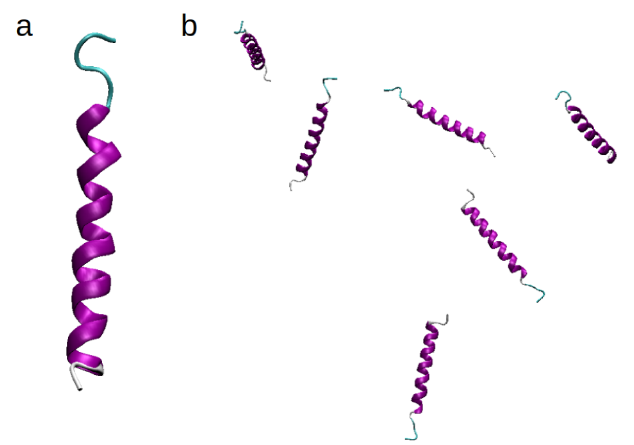

Figure 1. Starting configurations of (a) the glucagon molecule (PDB ID: 1GCN)[34] and (b) the simulated system comprising six glucagon monomers for the aggregation study. These visual representations were created using visual molecular dynamics (VMD).[44]

The simulations involved observing how glucagon aggregated in three different environments: pure water, water containing 10.7% (w/w) lactose, and water with 10.7% (w/w) 2-HPβCD. The water or water−cosolute solutions were described implicitly, as detailed in the Theoretical Background2.1.1 section.

To model the behavior of glucagon and its interaction with its surroundings, we used the generalized Born surface area model of AMBER 20 for simulating G^{el} and G^{np} in eq 1. Furthermore, the free energy of the transfer term $G^{tr}(c)$ was introduced as an external bias using PLUMED. To optimize computational efficiency and reduce the computational cost associated with the $G^{tr}(c)$ biasing force, a multiple time step approach was used[43] and, specifically, this term was added to every two integration steps.

In order to study the aggregation process, six glucagon molecules were randomly placed within a spherical cage of radius r_{sphere} = 14 nm, as depicted in Figure 1b. This configuration corresponded to a concentration of 3 g/L. A harmonic potential U_{sphere} was applied to prevent the peptides from drifting away from the borders of the spherical container.

$$\alpha_k = \begin{cases} k_{sphere}(|r_i - r_{center}| - r_{sphere})^2 & \text{if } |r_i - r_{center}| > r_{sphere} \\ 0 & \text{otherwise} \end{cases} \tag{5}$$

where r_i is the position of the center of mass of peptide i, while r_{center} is the position of the center of the sphere. k_{sphere} was set to 10 kcal/(mol nm^2).

During the production runs, simulations were conducted for a total of 300 ns. The initial 100 ns were designated as an equilibration period and were not considered for subsequent analyses. Only the last 200 ns of the simulation data were used for further analysis.

Langevin dynamics was employed to regulate the temperature at 298 K, with a collision frequency of 1.0 ps^{-1}. The SHAKE algorithm[45] was applied to restrict all bonds linking to hydrogen atoms, and a time step of 2.0 fs was used. The system's configuration was saved every 2 ps, and the center of mass translation and rotation were removed every 500 steps (1 ps). There were no cutoff values applied for handling Coulombic and Lennard-Jones interactions.

The $g_{k,sc}^{tr}(c)$ and $g_{bb}^{tr}(c)$ parameters, which will be utilized in eq 3, for the two distinct cosolutes under examination in this study, namely, lactose and HPβCD, were derived from all-atom explicit solvent simulations performed by employing the ADD force field.[46] Specifically, the values for HPβCD were obtained from our previous computational investigation,[30] and are listed in Table S2. The free energy of transfer terms for lactose was instead extracted as described in the Supporting Information.

2.2. Analysis of the Trajectories. *2.2.1. α-Helix Content.* The α-helix (α) content, as employed in the subsequent sections of this study, is defined as the count of six-residue segments within the peptide exhibiting an α-helical configuration,[47]

$$\alpha = \sum_k g[r_{dist}(\{R_i\}_{i\in\Omega_\mu}, \{R^0\})] \tag{6}$$

The summation runs over all possible segments contributing to the α-helix, while $\{R_i\}_{i\in\Omega\mu}$ represents the atomic coordinates of a specific set Ω_μ of six-residue fragments of the protein, and $g(r_{\text{dist}})$ is the following switching function,

$$g(r_{\text{dist}}) = \frac{1 - \left(\frac{r_{\text{dist}}}{r_0}\right)^8}{1 - \left(\frac{r_{\text{dist}}}{r_0}\right)^{12}} \quad (7)$$

A cutoff distance of r_0 = 0.08 nm was used, and r_{dist} represents the root-mean-square deviation from a reference α-helix structure denoted as $\{R^0\}$.

2.2.2. Hydrogen Bond Analysis. The number of hydrogen bonds within each system was also measured. For the detection of a hydrogen bond, a geometric criterion was applied, which required that the distance between the donor and acceptor was less than 0.30 nm and that the angle formed between the acceptor, hydrogen, and donor atoms was greater than 135°.

2.3. Experimental Validation. *2.3.1. Sample Preparation.* Glucagon samples (provided as lyophilized powder by Fresenius Kabi) were prepared by dissolving enough glucagon to prepare approximately 2 mL of 1 mg/mL in each of the following solutions at room temperature, and another set was prepared at 4 °C: water adjusted to pH 2.7 with HCl, 10.7% (w/v) lactose (Sigma 61339), and 10.7% (w/v) 2-hydroxypropyl-β-cyclodextrin (HPβCD Sigma 389145). The samples were immediately run on an MMS system, then incubated for 24 h at room temperature and at 4 °C, and run again. The list of samples analyzed is given in Table 1.

Table 1. Full List of Samples Analyzed[a]

sample, #	description
1	1 mg/mL glucagon dissolved in pH 2.7 water at RT
2	1 mg/mL glucagon dissolved in pH 2.7 water at 4 °C
3	1 mg/mL glucagon dissolved in 10.7% lactose at RT
4	1 mg/mL glucagon dissolved in 10.7% lactose at 4 °C
5	1 mg/mL glucagon dissolved in 10.7% HPβCD at RT
6	1 mg/mL glucagon dissolved in 10.7% HPβCD at 4 °C

[a]Each sample was then incubated at either room temperature (RT) or 4 °C overnight and run again after 24 h.

2.3.2. MMS Methods. Samples were run on a first-generation microfluidic modulation spectroscopy (AQS[3]pro MMS system, RedShiftBio, Boxborough, MA, USA) system with sweep scan functionality immediately after preparation, and again after 24 h incubation. MMS is an IR tool used to measure protein secondary structures. With the use of a quantum cascade laser as the light source and constantly modulating between the sample and the reference buffer, MMS can accurately measure aqueous samples at very low concentrations, even in complex or strongly absorbing backgrounds.

All samples were loaded in sample-reference buffer pairs in a 24-well plate. A backing pressure of 5 psi was used to move the samples into the flow cell (path length of 22.3 μm and temperature controlled to 25 °C), and a 1 Hz rate was used to take readings and modulate between the sample and the reference buffer. The laser scanned across the amide I band from 1588 to 1712 cm^{-1} and collected and averaged eight spectra per replicate. Three replicates were collected for each sample, and the data presented are the averages of all replicates.

Lysozyme was used as the model protein for comparison and baseline matching. Savitzky–Golay smoothing with a 19-wavenumber window was applied to the second derivative plot. The second derivative plot was inverted, and the baseline was subtracted to yield a similarity plot, which was used for Gaussian curve fitting. 11 Gaussian curves were used to quantitate the fractional contribution of secondary structures, as shown in the bar chart in Figure 5D.

3. RESULTS

3.1. In Silico Analysis. The average number of interpeptide hydrogen bonds between the glucagon molecules

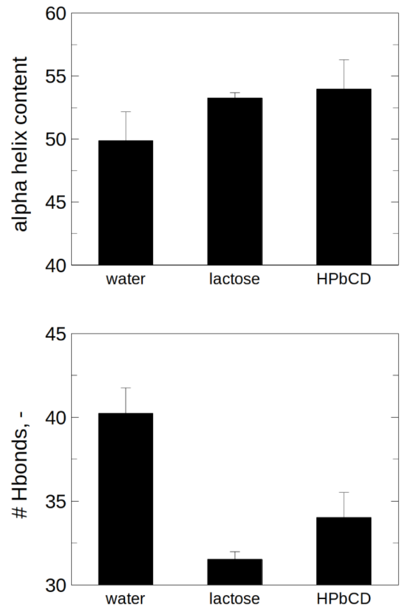

Figure 2. Average α-helical content (top graph) and number of interpeptide hydrogen bonds (bottom graph) for the three systems investigated. The error bars show one standard deviation as determined through the block averaging method.

and the average α-helical content were evaluated during the last 200 ns of the implicit solvent simulations. The results of this analysis are shown in Figure 2 where errors were estimated by block averaging. Briefly, the equilibrated trajectories were divided into four blocks, and the standard deviation was computed over the average values of the properties in each of the blocks.

We observed that both lactose and HPβCD increased the retention of α-helical content in glucagon and decreased the formation of hydrogen bonds between peptides when compared with glucagon in pure water. These results are noteworthy, because lactose and HPβCD typically exhibit opposing effects on protein conformations.

Lactose acted as a stabilizer, yielding a positive $g_{\text{bb}}^{\text{tr}}(c)$, while HP$\beta$CD had a slight denaturing effect, resulting in a negative $g_{\text{bb}}^{\text{tr}}(c)$. However, their overall impact on the aggregation propensity of glucagon was found to be similar.

Notably, the α-helical content of glucagon remained unchanged in the presence of cyclodextrin, contrary to expectations. Our interpretation of this finding is that HPβCD may act to prevent glucagon aggregation. Typically, aggregation leads to a loss of the secondary structure through protein–protein interactions. However, in the presence of HPβCD, these interactions may be reduced, thereby preserving the α-helical content. This hypothesis is supported by the observation of favorable interactions between HPβCD and the

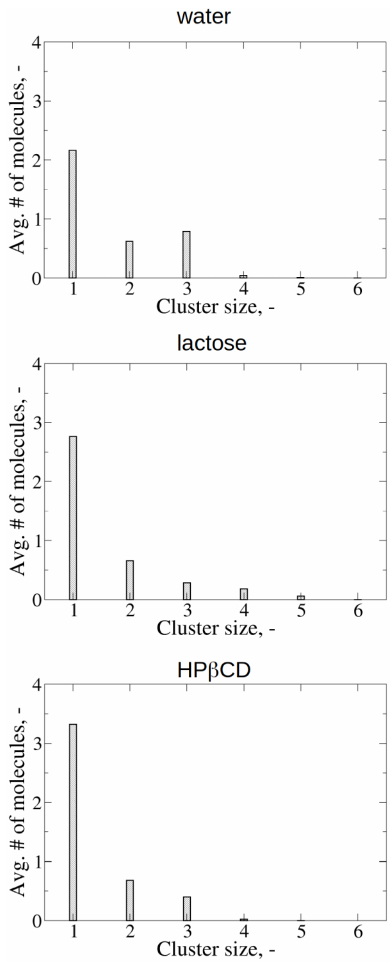

Figure 3. Average number of glucagon molecules within clusters in relation to the cluster size, as observed across all the solution conditions under investigation.

protein backbone, as indicated by the negative free energy of transfer values. Such interaction patterns align with those of classical denaturants, as discussed in relevant literature,[48,49] where denaturants typically reduce protein−protein interactions by interacting with the protein surface. Thus, these results suggest that HPβCD may exhibit denaturant-like properties, potentially preventing secondary structure loss, even at low concentrations.

These observations are corroborated by the average distribution of aggregate sizes recorded in the simulations, as shown in Figure 3. In the case of pure water, only two glucagon molecules were, on average, found in their monomeric state, while the remaining peptides tended to form higher-order clusters, especially dimers and trimers.

When either lactose or HPβCD was introduced, the number of glucagon molecules existing in the monomeric state increased to around three, with cyclodextrin exhibiting a more pronounced effect in preventing aggregation than lactose. Additionally, some tetramers and pentamers were sparsely populated in the presence of lactose, albeit with a low occurrence.

Lactose, acting as a stabilizer, tends to be preferentially excluded from the protein surface. As a result, lactose thermodynamically favors states that expose a reduced surface area such as the native protein fold (in comparison to the unfolded state) or multimeric aggregate species (in comparison to the monomeric, isolated form). This preference might elucidate why tetramers and pentamers were more frequently observed in the presence of lactose than in a pure water environment. Although lactose slightly promotes the formation of tetramers and pentamers compared to water, Figure 2 demonstrates that this oligomer formation does not result in a decrease in the α-helical content, nor does it increase the number of intermolecular hydrogen bonds between glucagon molecules. This result suggests that lactose, being preferentially excluded from the protein surface, shifts the equilibrium toward protein species that minimize surface area exposure. The native state is more compact than the unfolded one and is, therefore, stabilized.

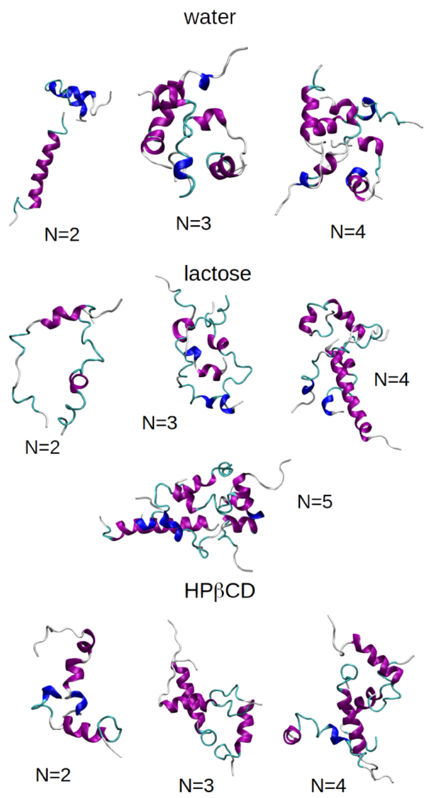

Figure 4. Most likely conformations of each cluster, encompassing all of the examined solution conditions. In this representation, α-helices are depicted in purple, 3_{10}-helices in blue, turns in cyan, and coils in white.

Similarly, native oligomers exposed less surface area than monomers and were thus also stabilized by preferentially excluded excipients like lactose. These observations imply that the oligomers might be linked by relatively weak forces, making them capable of reversibly converting to the monomeric state. The formation of reversible oligomers is commonly observed with excipients that function through the preferential exclusion mechanism such as lactose. Additionally, Figure 3 indicates that the average number of glucagon molecules in the monomeric state is higher in the presence of lactose than that in water, further suggesting that lactose hinders the irreversible aggregation of glucagon. If the unfolding process is the determining step for aggregation, then preferentially excluded excipients like lactose are beneficial in counteracting the aggregation cascade.

Figure 4 shows snapshots of the most likely aggregated conformations, as extracted from the implicit solvent

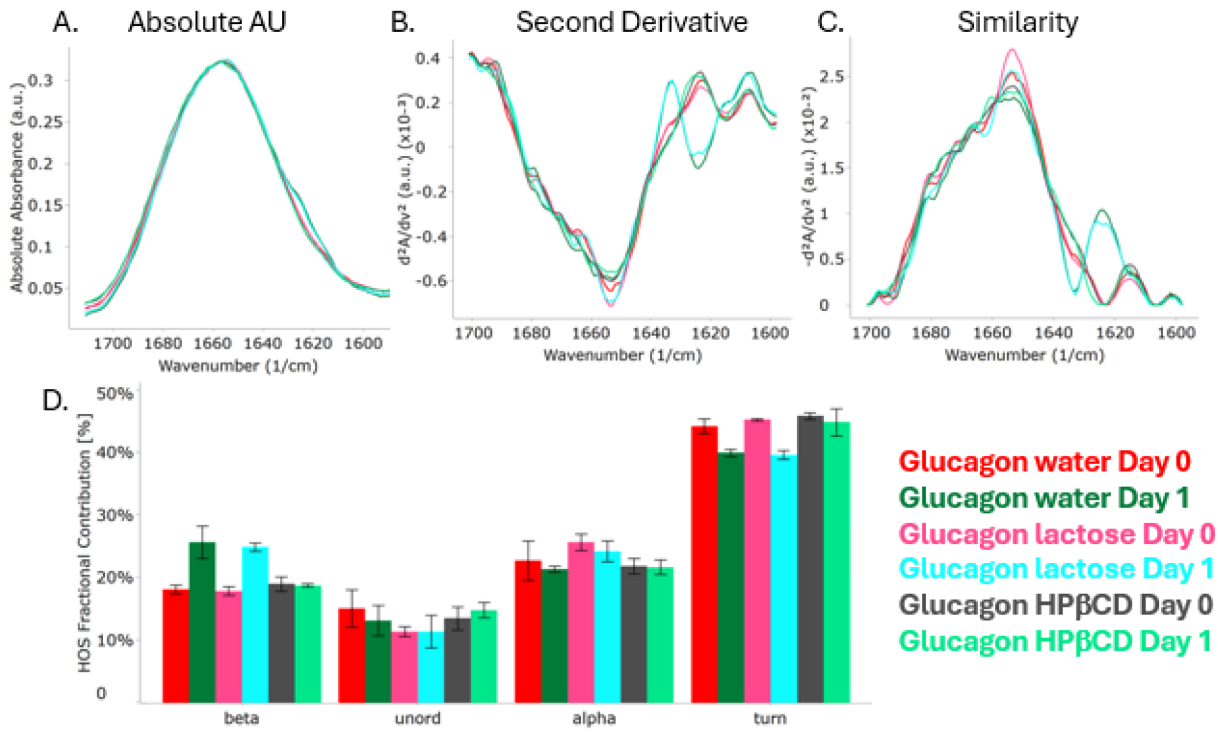

Figure 5. All samples were incubated at room temperature: A) The absolute absorbance spectra for each sample show a similar structure for the samples, where the main peak is located near 1656 cm^{-1}. B) Second derivative analysis reveals smaller disparities between the samples, specifically around 1620 cm^{-1}, where the samples in water and lactose after 24 h incubation show significant structural changes. C) A similarity plot is generated from the inverted and baselined-subtracted second derivative spectra to facilitate Gaussian curve fitting. D) The fractional contribution of secondary structures for glucagon under these six conditions shows that the samples in water and lactose, after 24 h incubation, had an increase in the β-sheet content typically associated with aggregation, and that the sample in HPβCD was resistant to the aggregation.

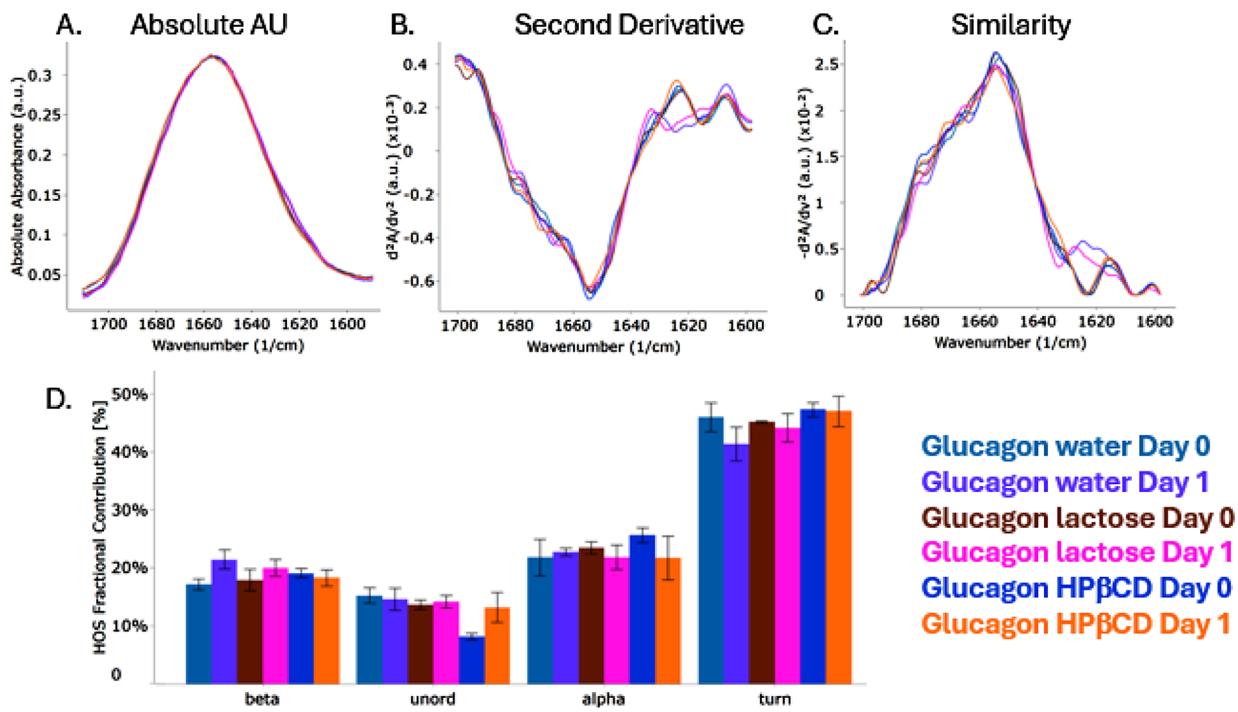

Figure 6. All samples were incubated at 4 °C: A) Absolute absorbance spectra have been baselined and normalized for concentration. B) Second derivative plots highlight regions of small changes, specifically the region near 1620 cm^{-1} indicating structural changes in the samples dissolved in water and lactose after 24 h incubation. C) The similarity plot is the inverted and baselined second derivative that was used for Gaussian curve fitting to get the higher order structure (HOS) percentages. D) The HOS bar chart shows that glucagon after 24 h in water increases the β-sheet content, consistent with aggregation. In the presence of 10.7% lactose, the increase in the β-sheet content is less, and in the presence of HPβCD, the β-sheet content does not increase after 24 h.

Table 2. Calculated Displacement Factors for Each Sample Run on MMS[a]

sample	displacement factor
water RT day 0	0.29
water RT day 1	0.16
water 4 °C day 0	0.29
water 4 °C day 1	0.25
lactose RT day 0	0.88
lactose RT day 1	0.49
lactose 4 °C day 0	1.01
lactose 4 °C day 1	0.84
HPβCD RT day 0	1.24
HPβCD RT day 1	1.10
HPβCD 4 °C day 0	1.18
HPβCD 4 °C day 1	1.34

[a]Glucagon in water displaces the least water, and glucagon in HPβCD displaces the most water.

simulations. These initial oligomeric forms of glucagon did not exhibit a significant β-sheet content. Intermolecular β-sheets likely form later during the aggregation process, in time scales that could not be reached by our molecular dynamics simulations. Instead, the first oligomers that we observed were primarily characterized by a reduced α-helical content compared to the native glucagon, and turn and coil structures served as connectors between different peptides within the clusters.

Drawing from these simulation results, it can be inferred that both lactose and, to an even greater extent, HPβCD foster the monomeric state of glucagon when compared to that of water. Given that lactose and HPβCD exhibit contrasting behaviors with lactose acting as a stabilizer and HPβCD as a denaturant, it is clear that their mechanisms of action differ.

Based on these findings, we hypothesize that denaturation and aggregation are closely interconnected phenomena in the case of glucagon. This hypothesis is substantiated by the snapshots of aggregated oligomers in Figure 4, where the helix content is at least partially lost upon aggregation. Consequently, we can postulate that lactose inhibits aggregation by promoting the folded conformation of glucagon. This excipient reduces the population of partially unfolded conformations, which are the species driving the aggregation process. As a result, this leads to a diminished tendency for aggregation and stabilization of the monomeric form.

The mechanism is different for HPβCD. As previously established and in accordance with prior findings, this cyclodextrin exhibits surfactant-like properties. Consequently, it impedes aggregation through its favorable interaction with the protein surface, which obstructs protein−protein interactions. This interference with protein−protein contacts diminishes the aggregation-induced loss of α-helical content, ultimately preserving the native secondary structure, as can be seen in Figure 2.

3.2. Experimental Validation. Experimental validation was carried out through MMS to corroborate the insights gained from previous molecular simulations. As determined by MMS, the native structures of glucagon when freshly dissolved in water, lactose, and HPβCD were mostly turn structures and an α-helix, which was expected from the MD simulations. After 24 h incubation at RT, the glucagon samples in water and lactose showed an increase in the β-sheet content, indicating instability and a propensity for aggregation (Figure 5).

Glucagon samples incubated at 4 °C in water and lactose (Figure 6) also showed an increase in the β-sheet content, but the extent was reduced, demonstrating that the colder temperature slowed the aggregation process. In addition, the increase in the β-sheet content in lactose was less pronounced than in water during 24 h incubation at 4 °C, suggesting that lactose tends to slow down the aggregation process. Interestingly, in the presence of HPβCD, glucagon did not undergo structural changes during 24 h incubation at either RT or 4 °C, showing that HPβCD is very effective at inhibiting aggregation. The ranking of glucagon stability within the tested formulations as determined via MMS (HPβCD > lactose > water) matches, therefore, the molecular dynamics simulation outputs.

As part of the MMS software, the "displacement factor" was calculated, which refers to the amount of buffer that is displaced by the protein, governed by the volume of the protein, and is separate from the structural measurements. Table 2 shows the calculated values for each sample. Glucagon dissolved in water displaced the least buffer, followed by lactose, and lastly, glucagon dissolved in HPβCD displaced the most buffer. This observation supports the hypothesis that HPβCD inhibits aggregation by binding to the external surface of glucagon, which restricts the protein−protein interactions responsible for aggregation.

4. CONCLUSIONS

Through a synergy of in silico simulations and experimental validation, we unraveled the intricate mechanisms of glucagon aggregation and identified strategies to mitigate its adverse effects.

The in silico simulations revealed that lactose and 2-HPβCD, two excipients with opposing behaviors, play crucial roles in modulating glucagon's aggregation propensity. Lactose, as a stabilizer, fosters the monomeric state of glucagon by increasing its α-helical content, while 2-HPβCD, functioning as a surfactant, impedes aggregation by inhibiting protein−protein interactions. These findings not only enhance our understanding of the underlying mechanisms but also offer actionable strategies for therapeutic peptide development.

To validate the in silico results, we employed microfluidic modulation spectroscopy (MMS), demonstrating that glucagon, in the presence of 2-HPβCD, remains structurally stable, affirming the antiaggregation potential of this excipient. Additionally, the displacement factor analysis further supported our hypothesis by showing that 2-HPβCD inhibits aggregation through its interaction with the external surface of glucagon, hindering protein−protein interactions. Lactose is less effective than 2-HPβCD at stabilizing glucagon, and a moderate effect of this excipient is observed in the MMS results only during incubation at 4 °C.

These results suggest that linear saccharides may stabilize glucagon similarly to lactose, though the extent of stabilization is likely dependent on the specific molecule considered. Cyclodextrin, by contrast, appears to prevent glucagon aggregation through its surfactant-like properties. Consequently, we anticipate that surfactants may exhibit a similar mechanism of action, with the degree of stabilization varying based on the specific surfactant used.

This research provides essential insights into the multifaceted world of glucagon aggregation and presents a blueprint for addressing this formidable challenge in therapeutic peptide development. By better understanding the dynamics of peptide aggregation, we move one step closer to the development of safe and effective therapeutic peptides, offering hope in the quest to combat both severe hypoglycemia and neurodegenerative diseases. The limitations of the implicit solvation method used in this study are acknowledged, particularly the restricted availability of transfer free energy data, which limits the number of formulations that can be simulated. Additionally, this method cannot be easily extended to coarse-grained simulations. Future research should prioritize creating a more extensive data set of transfer free energies for relevant excipients and aim to extend the proposed approach for coarse-grained simulations. Addressing these limitations will enhance the robustness and applicability of the findings, providing a more comprehensive understanding of excipient behavior in preventing glucagon aggregation.

■ ASSOCIATED CONTENT

Supporting Information

The Supporting Information is available free of charge at https://pubs.acs.org/doi/10.1021/acs.molpharmaceut.4c00038.

Explicit solvent simulations for lactose and values of transfer free energies employed for the implicit solvent runs (PDF)

■ AUTHOR INFORMATION

Corresponding Authors

Roberto Pisano − *Department of Applied Science and Technology, Politecnico di Torino, Torino IT-10129, Italy*; orcid.org/0000-0001-6990-3126; Email: roberto.pisano@polito.it

Antonio Ricci − *Fresenius Kabi iPSUM, Cassina de Pecchi IT-20081, Italy*; Email: antonio.ricci@fresenius-kabi.com

Authors

Andrea Arsiccio − *Department of Applied Science and Technology, Politecnico di Torino, Torino IT-10129, Italy*; Present Address: Coriolis Pharma Research, 18B Fraunhoferstraße, DE-82152, Martinsried, Germany

Valerie Collins − *Redshift Bioanalytics, Boxborough, Massachusetts MA-01719, United States*

Patrick King − *Redshift Bioanalytics, Boxborough, Massachusetts MA-01719, United States*

Marco Macis − *Fresenius Kabi iPSUM, Cassina de Pecchi IT-20081, Italy*

Walter Cabri − *Fresenius Kabi iPSUM, Cassina de Pecchi IT-20081, Italy; Center for Chemical Catalysis Department of Chemistry "Giacomo Ciamician", University of Bologna, Bologna 40126, Italy*

Complete contact information is available at: https://pubs.acs.org/10.1021/acs.molpharmaceut.4c00038

Author Contributions

#R.P., A.A., and V.C. contributed equally to the manuscript editing.

Notes

The authors declare no competing financial interest.

■ ACKNOWLEDGMENTS

Computational resources were provided by HPC@POLITO, a project of Academic Computing within the Department of Control and Computer Engineering at the Politecnico di Torino (http://hpc.polito.it), and by CINECA under the ISCRA initiative (ProtImp- HP10C4PRAT).

■ REFERENCES

(1) Sipe, J. D.; Cohen, A. S. Review: History of the amyloid fibril. *J. Struct. Biol.* **2000**, *130* (2−3), 88−98.

(2) Chiti, F.; Dobson, C. M. Protein misfolding, functional amyloid, and human disease. *Annu. Rev. Biochem.* **2006**, *75*, 333−366.

(3) Selkoe, D. J.; Hardy, J. The amyloid hypothesis of Alzheimer's disease at 25 years. *EMBO Mol. Med.* **2016**, *8* (6), 595−608.

(4) Long, J. M.; Holtzman, D. M. Alzheimer disease: An update on pathobiology and treatment strategies. *Cell* **2019**, *179* (2), 312−339.

(5) Westermark, P.; Andersson, A.; Westermark, G. T. Islet amyloid polypeptide, islet amyloid, and diabetes mellitus. *Physiol. Rev.* **2011**, *91*, 795−826.

(6) Boyer, S. K.; Laine, E. S. Glucagon as a potential biopharmaceutical for treating hypoglycemia. *Diabetes* **1984**, *33* (8), 757−765.

(7) Marassi, V.; Macis, M.; Giordani, S.; Ferrazzano, L.; Tolomelli, A.; Roda, B.; Zattoni, A.; Ricci, A.; Reschiglian, P.; Cabri, W. Application of Af4-multidetection to Liraglutide in its formulation: Preserving and representing native aggregation. *Molecules* **2022**, *27*, 5485.

(8) Bromer, W. W.; Sinn, L. G.; Chakrabarti, S. Therapeutic use of glucagon. *Drug Develop. Res.* **1983**, *3* (5), 473−485.

(9) Unson, C. G. Molecular determinants of glucagon receptor signaling. *Peptide Sci.* **2002**, *66*, 218−235.

(10) Hall-Boyer, K.; Zaloga, G. P.; Chernow, B. Glucagon: Hormone or therapeutic agent? *Crit. Care Med* **1984**, *12*, 584−589.

(11) Bromer, W. W. Chemical characteristics of glucagon, In *Glucagon I*; 1st ed. Lefèbvre, P. J., Ed.; Springer, Berlin Heidelberg, 1983 pp. 122.

(12) FDA. Glucagon for injection: Highlights of prescribing information, *U.S. Food and Drug Administration*, 2022.https://www.accessdata.fda.gov/drugsatfda_docs/label/2022/201849s013lbl.pdf.

(13) Onoue, S.; Ohshima, K.; Debari, K.; Koh, K.; Shioda, S.; Iwasa, S.; Kashimoto, K.; Yajima, T. Mishandling of the therapeutic peptide glucagon generates cytotoxic amyloidogenic fibrils. *Pharm. Res.* **2004**, *21*, 1274−1283.

(14) Pedersen, J. S. The nature of amyloid-like glucagon fibrils. *J. Diabetes Sci. Technol.* **2010**, *4*, 1357−1367.

(15) De Jong, K. L.; Incledon, B.; Yip, C. M.; DeFelippis, M. R. Amyloid fibrils of glucagon characterized by high-resolution atomic force microscopy. *Biophys. J.* **2006**, *91*, 1905−1914.

(16) Zhou, X.; Tan, J.; Zheng, L.; Pillai, S.; Li, B.; Xu, P.; Zhang, B.; Zhang, Y. The opposite effects of Cu(II) and Fe(III) on the assembly of glucagon amyloid fibrils. *RSC Adv.* **2012**, *2*, 5418−5423.

(17) Hoppe, C. C.; Nguyen, L. T.; Kirsch, L. E.; Wiencek, J. M. Characterization of seed nuclei in glucagon aggregation using light scattering methods and field-flow fractionation. *J. Biol. Eng.* **2008**, *2*, 10.

(18) Bakhtiani, P. A.; Caputo, N.; Castle, J. R.; El Youssef, J.; Carroll, J. M.; David, L. L.; Roberts, C. T., Jr; Ward, W. K. A novel, stable, aqueous glucagon formulation using ferulic acid as an excipient. *J. Diabetes Sci. Technol.* **2014**, *9*, 17−23.

(19) Košmrlj, A.; Cordsen, P.; Kyrsting, A.; Otzen, D. E.; Oddershede, L. B.; Jensen, M. H. A monomer-trimer model supports intermittent glucagon fibril growth. *Sci. Rep.* **2015**, *5*, 9005.

(20) Onoue, S.; Iwasa, S.; Kojima, T.; Katoh, F.; Debari, K.; Koh, K.; Matsuda, Y.; Yajima, T. Structural transition of glucagon in the concentrated solution observed by electrophoretic and spectroscopic techniques. *J. Chromatogr. A* **2006**, *1109*, 167−173.

(21) Pohl, R.; Li, M.; Krasner, A.; De Souza, E. Development of stable liquid glucagon formulations for use in artificial pancreas. *J. Diabetes Sci. Technol.* **2014**, *9*, 8−16.

(22) Chabenne, J. R.; DiMarchi, M. A.; Gelfanov, V. M.; DiMarchi, R. D. Optimization of the native glucagon sequence for medicinal purposes. *J. Diabetes Sci. Technol.* **2010**, *4*, 1322−1331.

(23) Oliveira, C. L. P.; Behrens, M. A.; Pedersen, J. S.; Erlacher, K.; Otzen, D.; Peder- Sen, J. S. A SAXS study of glucagon fibrillation. *J. Mol. Biol.* **2009**, *387*, 147−161.
(24) Stimple, S. D.; Kalyoncu, S.; Desai, A. A.; Mogensen, J. E.; Spang, L. T.; Asgreen, D. J.; Staby, A.; Tessier, P. M. Sensitive detection of glucagon aggregation using amyloid fibril-specific antibodies. *Biotechnol. Bioeng.* **2019**, *116*, 1868−1877.
(25) Serno, T.; Carpenter, J. F.; Randolph, T. W.; Winter, G. Inhibition of agitation- induced aggregation of an IgG-antibody by hydroxypropyl-β-cyclodextrin. *J. Pharm. Sci.* **2010**, *99*, 1193−1206.
(26) Tavornipas, S.; Tajiry, S.; Hirayama, F.; Arima, H.; Uekama, K. Effects of Hydrophilic cyclodextrins on aggregation of recombinant human growth hormone. *Pharm. Res.* **2004**, *21*, 2369−2376.
(27) Serno, T.; Härtl, E.; Besheer, A.; Miller, R.; Winter, G. The role of polysorbate 80 and HPβCD at the air-water interface of IgG solutions. *Pharm. Res.* **2013**, *30*, 117−130.
(28) Timasheff, S. Protein-solvent preferential interactions, protein hydration, and the modulation of biochemical reactions by solvent components. *Proc. Natl. Acad. Sci. U. S. A.* **2002**, *99*, 9721−9726.
(29) Timasheff, S. The control of protein stability and association by weak interactions with water: How do solvents affect these processes? *Annu. Rev. Biophys. Biomol. Struct.* **1993**, *22*, 67−97.
(30) Arsiccio, A.; Rospiccio, M.; Shea, J.-E.; Pisano, R. Force field parameterization for the description of the interactions between hydroxypropyl-β-cyclodextrin and proteins. *J. Phys. Chem. B* **2021**, *125*, 7397−7405.
(31) Oliveri, V.; Vecchio, G. Cyclodextrins as protective agents of protein aggregation: An overview. *Chem.-Asian J.* **2016**, *11* (5), 1648−1657.
(32) Niccoli, M.; Oliva, R.; Castronuovo, G. Cyclodextrin−protein interaction as inhibiting factor against aggregation. *J. Therm. Anal. Calorim.* **2017**, *127*, 1491−1499.
(33) Arsiccio, A.; Ganguly, P.; Shea, J.-E. A transfer free energy based implicit solvent model for proteins simulations in solvent mixtures: Urea-induced denaturation as a case study. *J. Phys. Chem. B* **2022**, *126* (24), 4472−4482.
(34) Qiu, D.; Shenkin, P. S.; Hollinger, F. P.; Still, W. C. The GB/SA continuum model for solvation. A fast analytical method for the calculation of approximate born radii. *J. Phys. Chem. A* **1997**, *101*, 3005−3014.
(35) Onufriev, A.; Bashford, D.; Case, D. A. Exploring protein native states and large-scale conformational changes with a modified generalized born model. *Proteins: Struct., Funct., Bioinf.* **2004**, *55*, 383−394.
(36) Bradley, D. J.; Pitzer, K. S. Thermodynamics of electrolytes. 12. Dielectric properties of water and Debye-Hueckel parameters to 350 °C and 1 kbar. *J. Phys. Chem.* **1979**, *83*, 1599−1603.
(37) Sitkoff, D.; Sharp, K. A.; Honig, B. Accurate calculation of hydration free energies using macroscopic solvent models. *J. Phys. Chem.* **1994**, *98*, 1978−1988.
(38) Hasel, W.; Hendrickson, T. F.; Still, W. C. A rapid approximation to the solvent accessible surface areas of atoms. *Tetrahedron Comput. Methodol.* **1988**, *1*, 103−116.
(39) Lindor-Larsen, K.; Piana, S.; Palmo, K.; Maragakis, P.; Klepeis, J. L.; Dror, R. O.; Shaw, D. E. Improved side-chain torsion potentials for the Amber $ff_{99}SB$ protein force field. *Proteins: Struct., Funct., Bioinf.* **2010**, *78*, 1950−1958.
(40) Sasaki, K.; Dockerill, S.; Adamiak, D. A.; Tickle, I. J.; Blundell, T. X-ray analysis of glucagon and its relationship to receptor binding. *Nature* **1975**, *257*, 751−757.
(41) Pearlman, D. A.; Case, D. A.; Caldwell, J. W.; Ross, W. S.; Cheatham, T. E.; De- Bolt, S.; Ferguson, D.; Seibel, G.; Kollman, P. AMBER, a package of computer pro- grams for applying molecular mechanics, normal mode analysis, molecular dynam- ics and free energy calculations to simulate the structural and energetic properties of molecules. *Comput. Phys. Commun.* **1995**, *91*, 1−41.
(42) Tribello, G. A.; Bonomi, M.; Branduardi, D.; Camilloni, C.; Bussi, G. PLUMED 2: New feathers for an old bird. *Comput. Phys. Commun.* **2014**, *185*, 604−613.
(43) Ferrarotti, M. J.; Bottaro, S.; Pérez-Villa, A.; Bussi, G. Accurate multiple time step in biased molecular simulations. *J. Chem. Theory Comput.* **2015**, *11*, 139−146.
(44) Humphrey, W.; Dalke, A.; Schulten, K. VMD: Visual molecular dynamics. *J. Mol. Graphics* **1996**, *14*, 33−38.
(45) Ryckaert, J.-P.; Ciccotti, G.; Berendsen, H. J. Numerical integration of the cartesian equations of motion of a system with constraints: Molecular dynamics of n-alkanes. *J. Comput. Phys.* **1977**, *23*, 327−341.
(46) Arsiccio, A.; Ganguly, P.; La Cortiglia, L.; Shea, J.-E.; Pisano, R. ADD force field for sugars and polyols: Predicting the additivity of protein-osmolyte interaction. *J. Phys. Chem. B* **2020**, *124*, 7779−7790.
(47) Pietrucci, F.; Laio, A. A collective variable for the efficient exploration of protein beta-sheet structures: Application to SH3 and GB1. *J. Chem. Theory. Comput.* **2009**, *5*, 2197−2201.
(48) Auton, M.; Holthauzen, L. M. F.; Bolen, D. W. Anatomy of energetic changes accompanying urea-induced protein denaturation. *Proc. Natl. Acad. Sci. U. S. A.* **2007**, *104*, 15317−15322.
(49) Rospiccio, M.; Arsiccio, A.; Winter, G.; Pisano, R. The role of cyclodextrins against interface-induced denaturation in pharmaceutical formulations: A molecular dynamics approach. *Mol. Pharmaceutics* **2021**, *18*, 2322−2333.